Preparation, Biodistribution, and Small Animal PET of ^{45}Ti-Transferrin

Amy L. Vavere, PhD[1,2]; and Michael J. Welch, PhD[1–3]

[1]Mallinckrodt Institute of Radiology, Washington University School of Medicine, St. Louis, Missouri; [2]Department of Chemistry, Washington University in St. Louis, St. Louis, Missouri; and [3]Alvin J. Siteman Cancer Center, Washington University School of Medicine, St. Louis, Missouri

Investigation of ^{45}Ti-transferrin was pursued to provide insight into the mechanism of action of titanocene dichloride, a chemotherapeutic agent currently in clinical trials. **Methods:** Plasma protein-binding studies of processed ^{45}Ti were performed by solubilizing the ^{45}Ti residue in 0.05N HCl, of which 1.22 MBq (33 μCi) in 10 μL were added to 250 μL of dog plasma. ^{45}Ti-Transferrin was prepared by redissolving the processed ^{45}Ti in 25 μmol/L apotransferrin or by in vivo incorporation through preparation and introduction of ^{45}Ti-citrate. Biodistribution studies were performed on normal Sprague–Dawley rats and EMT-6 tumor-bearing BALB/c mice with ^{45}Ti-transferrin coinjected with ^{67}Ga-citrate for direct comparison. microPET was performed on mice bearing EMT-6 tumors and the images were analyzed for tumor-to-muscle uptake ratios. **Results:** Direct labeling of apotransferrin in situ with ^{45}Ti was achieved as well as in vivo incorporation by 2 h after injection with ^{45}Ti-citrate. The biodistribution of ^{45}Ti-transferrin and ^{67}Ga-citrate showed similar trends. In Sprague–Dawley rats, initial blood uptake was higher for the ^{45}Ti-transferrin, whereas bone uptake increased more for the ^{67}Ga-citrate. EMT-6 tumor uptake in both cases was relatively high (14.6 ± 1.83 %ID/g for ^{45}Ti and 8.72 ± 0.98 %ID/g for ^{67}Ga [%ID/g = percentage injected dose per gram]) and remained elevated even out to 24 h after injection. The tumor-to-muscle ratio of the ^{67}Ga-citrate reached 6.7 at 24 h, whereas the ratio of the ^{45}Ti-transferrin increased to 4.3 at this time point. Uptake of ^{45}Ti-transferrin was visualized in the EMT-6 murine mammary carcinoma tumor with microPET. In all cases, the tumor was clearly delineated from the surrounding tissue with tumor-to-muscle ratios on the order of 1.6. **Conclusion:** ^{45}Ti forms a complex with apotransferrin that remains intact in vivo. Results of the biodistribution in mice showed that the tumor had increased uptake compared with nontarget organs (e.g., muscle). The microPET images of tumor-bearing mice clearly delineate the tumors from the surrounding tissue. Comparison of the data suggests that tissue uptake is similar whether injecting ^{45}Ti-transferrin directly or as ^{45}Ti-citrate, which transchelates to transferrin before the time of imaging.

Key Words: ^{45}Ti; transferrin; microPET

J Nucl Med 2005; 46:683–690

Received Aug. 13, 2004; revision accepted Nov. 2, 2004.

For correspondence or reprints contact: Michael J. Welch, PhD, Mallinckrodt Institute of Radiology, Washington University Medical School, 510 S. Kingshighway Blvd., Campus Box 8225, St. Louis, MO 63110.

E-mail: WelchM@mir.wustl.edu

Titanium(IV) complexes have been shown to exhibit high antitumor activity against a wide range of tumors (*1*). One of these compounds, titanocene dichloride, is currently in phase II clinical trials as an anticancer agent (*2,3*). Titanocene dichloride is effective against cisplatin-resistance cancers and with fewer toxic side effects. In contrast to the many areas of toxicity of cisplatin, titanocene dichloride appears to show only toxicity in the liver when given in therapeutic doses (*4,5*).

The specific pathway of transport of the pharmaceutical to tumor cells remains unclear, but numerous studies have demonstrated that titanium accumulates in nucleic acid–rich regions of the nucleus (*6,7*). Further elucidation of the mechanism of action of these compounds remains difficult due to their rapid hydrolysis under physiologic conditions (*8*). It has been demonstrated that Ti(IV) is readily taken up by human transferrin from titanocene dichloride (*9*). Transferrin is an iron-binding protein that shuttles iron between sites of uptake and utilization. This 80-kDa protein is comprised of 678 amino acids divided into 2 homologous lobes that each have an individual binding site deep inside a cleft. Normally, only 30% of transferrin is saturated with iron in vivo, leaving it available for the binding and transport of other metals. This protein may act as a natural carrier for anticancer drugs since tumor cell surfaces are known to contain high levels of transferrin receptors (*10,11*).

The metal-binding capabilities of transferrin have been investigated with >30 different metals and anions (*12*). Although no metal, with a known binding constant, binds as strongly as the endogenous iron, many are incorporated rather easily and remain bound for hours or days under physiologic conditions. Titanium-transferrin was first reported in 1998 (*13*) and confirmed by another group using similar methods in the following year (*14*). These results show that on titration with Ti(IV)citrate, apotransferrin is able to bind 2 atoms of Ti(IV). Through nuclear magnetic resonance studies, titanium was shown to be bound in the specific iron-binding site by association with tyrosines known to be involved in each of the 2 lobes of the protein.

Ga(III) and Ru(III) used in cancer imaging agents have been shown to use transferrin for transport (*15,16*). ^{67}Ga-

Citrate has long been used as a tracer for soft-tissue infection and non-Hodgkin's lymphoma for SPECT. Once injected, the gallium binds to apotransferrin and is distributed via the transferrin receptor pathway and other routes. The complex mechanism of accumulation of ^{67}Ga in tumors is affected by the blood supply and other iron-binding proteins as well as transferrin (*17*). Several studies have investigated this mechanism in detail using ^{67}Ga and EMT-6 mouse mammary carcinoma cells, known to express high levels of transferrin receptors (*18–22*). ^{68}Ga, a positron emitter with a 68-min half-life ($t_{1/2}$), is also used in the same formulation for PET (*23,24*).

^{45}Ti has a $t_{1/2}$ of 3.09 h and 85% of its decay occurs by positron emission. The high positron branching ratio and an $E_{\beta^+_{max}}$ of 1.04 MeV make ^{45}Ti a suitable candidate for PET. Ishiwata et al. investigated ^{45}Ti as a potential metal for labeling pharmaceuticals for PET by forming complexes with diethylenetriaminepentaacetic acid (DTPA), citric acid, and human serum albumin (*25,26*). However, these studies were published >10 y ago and, to our knowledge, this endeavor has not been pursued any further. The complicated radiochemistry and rapid oxidation of the metal in air continue to be major challenges to the development of ^{45}Ti compounds.

This article reports the radiochemical labeling strategy, biodistribution, and microPET of ^{45}Ti-transferrin. Outlining the uptake and transport of ^{45}Ti by transferrin will establish a new paradigm for the investigation of titanium anticancer drugs using radionuclidic techniques. Future studies may use this work as a basis for comparison to confirm the involvement of transferrin as a carrier for titanium from titanium-containing pharmaceuticals. These results suggest that titanium transferrin alone may produce effects comparable to the introduction of organometallic titanium complexes; this would implicate such complexes as prodrugs for delivery of titanium to cells by transferrin. ^{45}Ti-Transferrin could also act as a new imaging agent with better resolution than ^{68}Ga-citrate. ^{68}Ga has a maximum positron energy of 1.90 MeV, resulting in a less-resolved image using microPET when compared with ^{45}Ti (1.04 MeV) and a higher dose imparted to the subject.

MATERIALS AND METHODS

Unless otherwise stated, all chemicals were purchased from Aldrich Chemical Co., Inc. All solutions were prepared using distilled, deionized water (Milli-Q, Millipore Corp.; >18-MΩ resistivity). Radioactive samples were analyzed in a radioisotope calibrator (Capintec, Inc.) for determination of megabecquerels (millicuries) and a Beckman 8000 γ-counter for counts per minute. Radionuclidic purity was determined by analysis with a Canberra multichannel analyzing γ-spectrometer. Centrifugation was performed on a Sorvall Superspeed RC2-B Centrifuge refrigerated to 4°C. Fast-protein liquid chromatography (FPLC) was performed on an Amersham Pharmacia FPLC System, using a Superose 12 HR 10/30 size-exclusion column, 20 mmol/L *N*-(2-hydroxyethyl)piperazine-*N*′-(2-ethanesulfonic acid) (HEPES)/150 mmol/L NaCl, pH 7.3, as the mobile phase and a flow rate of 0.5 mL/min. ^{67}Ga-Citrate was obtained from PETNet. Small animal PET was performed on a microPET-R4 scanner (Concorde Microsystems, Inc.).

^{45}Ti

^{45}Ti was prepared as previously described (*27*). Briefly, a ^{nat}Sc foil target (thickness = 0.250 mm) was bombarded with ~14.7-MeV protons on a CS-15 cyclotron (Cyclotron Corp.). The ^{nat}Sc (p,n) ^{45}Ti nuclear reaction produced ^{45}Ti with an average decay-corrected yield of 421.8 MBq/μA·h (11.4 μCi/μA·h) and 2,109 MBq (57 mCi). The target was then dissolved in 2 mL 6N HCl and applied to a cation-exchange column containing AG50W-X8 resin (1.9 × 13 cm, 100–200 mesh). ^{45}Ti was eluted in 6N HCl (Alfa Aesar; diluted from 12N HCl) with 92.4% recovery. The HCl was removed by evaporation with heating under a stream of nitrogen, and the radionuclidic purity was determined to be 99.8% by analysis with a multichannel analyzing γ-spectrometer.

^{45}Ti Plasma Binding

Plasma protein-binding studies of the processed ^{45}Ti were performed as a preliminary test of feasibility. A 1.0-mL aliquot of dog blood was heparinized and centrifuged at 5,000 rpm for 5 min to separate the plasma from the red blood cells. The ^{45}Ti residue was dissolved in 0.05N HCl, of which 1.22 MBq (33 μCi) in 10 μL were added to 250 μL of plasma. Inversion of the vial several times ensured adequate mixing. The solution was then centrifuged in an Eppendorf filter (Brinkmann) with a molecular weight cutoff of 10,000 at 4,000 rpm until 80% of the solution passed through the filter. The amount of radioactivity in the eluent and on the filter was determined. An experiment was also performed by adding 5.92 MBq (160 μCi) to 1.5 mL of dog plasma and analysis by radio-FPLC after a 10-min, room temperature incubation.

^{45}Ti-Transferrin

The ^{45}Ti residue was dissolved in 25 μmol/L apotransferrin (murine, 99.8%) and 50 mmol/L HEPES/150 mmol/L NaCl buffer at 10 μg for each 37 MBq (1 mCi) of activity. All solutions contained freshly prepared 5 mmol/L bicarbonate as the synergistic anion for effective binding to apotransferrin. After a 5- to 60-min incubation period at room temperature, low-molecular-weight impurities, including unbound titanium, were removed using 1 of 2 methods. The ^{45}Ti-transferrin solution was either eluted through a PD-10 column (Amersham Biosciences) following the included protocol or centrifuged through a YM-30 Centricon tube (Millipore Corp.) at 5,000 rpm for 30 min and collected in the desired volume for further studies. A control experiment attempted ^{45}Ti binding to holotransferrin (iron-saturated transferrin) following the same methods outlined for the apotransferrin. Radio-FPLC was performed to determine the binding efficiency of ^{45}Ti to transferrin.

Further purification of the purchased protein was pursued before labeling in an attempt to improve labeling reproducibility. The apotransferrin was dissolved at 1 mg/mL in 50 mmol/L HEPES/150 mmol/L NaCl buffer. This solution was centrifuged in a YM-30 Centricon tube at 5,000 rpm for 30 min. Two milliliters of buffer were added to the tube and centrifuged at 5,000 rpm for 30 min. Buffer washing was repeated in triplicate, and the protein solution was collected in 300 μL by inversion of the tube and a brief (5 min) centrifugation at 5,000 rpm. This procedure would serve to remove any low-molecular-weight impurities before radiolabeling.

In vivo incorporation into transferrin was also attempted by the preparation and injection of ^{45}Ti-citrate. The ^{45}Ti residue was dissolved in 25 μmol/L ammonium citrate (100 μL). After a 30-min incubation period at room temperature, radio-FPLC was performed to determine the binding efficiency of ^{45}Ti to citrate. The solution was diluted with saline to a concentration of 7.4 MBq (200 μCi) in 100 μL, which was injected into each of 2 female BALB/c mice for binding analysis. At 2 h after injection, the mice were sacrificed and their blood was removed, heparinized, and centrifuged. The plasma was then analyzed by radio-FPLC to assess transferrin incorporation.

Biodistribution

All animal experiments were performed in compliance with the Guidelines for the Care and Use of Research Animals established by Washington University's Animal Studies Committee. A normal biodistribution was performed on male Sprague–Dawley rats (500–600 g) using ^{45}Ti dissolved in 0.05N HCl and diluted in 50 mmol/L HEPES-buffered saline ($n = 3$). After anesthetizing with isoflurane (2%), each animal was injected with 0.37 MBq (10 μCi) in 100 μL administered by bolus injection via the tail vein. Animals were allowed access to food and water ad libitum. The animals were sacrificed at selected time points after injection, and blood, lung, liver, spleen, kidney, muscle, and fat were removed, weighed, and counted for radioactivity accumulation. The percentage injected dose per gram (%ID/g) and percentage injected dose per organ (%ID/organ) were calculated by comparison to a weighed, counted standard solution.

In the ^{45}Ti-transferrin biodistribution studies, ^{67}Ga-citrate (^{67}Ga $t_{1/2} = 78$ h) was coinjected for comparison since it is known to be transported by transferrin. The γ-emissions of ^{67}Ga are at lower energies (94.4, 102.9, 309.8, and 403.2 keV) than the 511-keV emission of ^{45}Ti; therefore, the activity in each organ could be counted in a separate window for each isotope as well as allowing time for decay of ^{45}Ti before counting of ^{67}Ga.

^{45}Ti-Transferrin (1.11 MBq [30 μCi]) was coinjected into healthy, female Sprague–Dawley rats (500–600 g) with 0.37 MBq (10 μCi) ^{67}Ga-citrate. Harvested tissues included blood, lung, liver, spleen, kidney, muscle, fat, heart, brain, and bone. Organs were collected at 10 min and 2, 4, and 7 h ($n = 4$). These tissues were weighed and counted for ^{45}Ti and ^{67}Ga on the γ-counter along with a standard of the injected doses for comparison. Two separate windows were used for counting to separate the ^{67}Ga γ-emissions from ^{45}Ti. Decay-corrected uptakes were calculated as %ID/g and %ID/organ.

Female BALB/c mice (20–30 g) were implanted in the hind flank with 6×10^5 EMT-6 murine mammary carcinoma cells in suspension (100 μL) with >90% viability. The tumors were allowed 7 d of growth before the biodistribution study, at which point 0.74 MBq (20 μCi) ^{45}Ti-transferrin and 0.37 MBq (10 μCi) ^{67}Ga-citrate were coinjected into each mouse intravenously via the tail vein. Biodistributions were assessed at 2, 4, and 24 h after injection. Tissues harvested were blood, lung, liver, spleen, kidney, gallbladder, muscle, fat, heart, brain, bone, and tumor. These tissues were weighed and counted on the γ-counter with a standard of the injected dose for comparison. Decay-corrected uptakes were calculated as %ID/g and %ID/organ.

microPET

Single-position, whole-body imaging of ^{45}Ti-transferrin was performed on 2 tumor models using microPET. Mice were imaged individually or in pairs in a supine position in a specially designed bed. The bed was placed near the center of the field of view of the microPET scanner, where the highest image resolution and sensitivity are available. Imaging was performed in 15-min static sessions, with a collection of 600 frames per second. Isoflurane (2%) was used as an inhaled anesthetic to induce and maintain anesthesia during imaging.

An individual female BALB/c mouse was implanted in the right and left flank with 6×10^5 EMT-6 mouse mammary carcinoma cells in 100 μL with >90% viability. The tumors were allowed 14 d of growth before preliminary imaging with injection of 27.72 MBq (750 μCi) ^{45}Ti-transferrin.

After tumors were visualized by the preliminary imaging, 8 female BALB/c mice were implanted at the nape of the neck with 6×10^5 EMT-6 mouse mammary carcinoma cells in 100 μL with >90% viability. The tumors were used after 14 d of growth before imaging. Six of the mice with the largest tumors were imaged in pairs at 2 and 4 h after injection of ~7.4 MBq (200 μCi) ^{45}Ti-transferrin or ^{45}Ti-citrate.

The microPET images were evaluated by analysis of the standardized uptake value (SUV) of the tumor and nontarget organ (muscle) using ASIPRO software (Concorde MicroSystems, Inc.). The average radioactivity concentration within the tumor or tissue was obtained from the average pixel values reported in becquerels per milliliter (nCi/mL) within regions of interest (ROIs) drawn around the entire tumor or tissue on multiple, consecutive transaxial image slices. The SUV was calculated by dividing this value, the decay-corrected activity per unit volume of tissue (Bq/mL [nCi/mL]), by the injected activity per unit of body weight (Bq/g [nCi/g]). SUVs were compared with obtain a tumor-to-muscle ratio.

RESULTS

^{45}Ti Plasma Binding

In the preliminary plasma-binding study, ^{45}Ti was added to dog plasma to assess protein-binding capability. Virtually no activity was found in the eluent fraction, and all (>99%) of the ^{45}Ti was associated with the proteins in plasma, above the 10,000-Da filter.

Plasma-binding capability by ^{45}Ti was further analyzed using size-exclusion radio-FPLC. After a 10-min incubation period, the ultraviolet (UV) trace shows 3 mass peaks due to elution of proteins in the plasma. The radioactive trace shows a single radioactive peak matching the UV retention volume of a single protein in the plasma sample (Fig. 1) at 12.4 mL. After comparison with an elution profile of transferrin, this retention volume was determined to be that of transferrin.

^{45}Ti-Transferrin

Direct labeling of apotransferrin in situ with ^{45}Ti was achieved. Radio-FPLC analysis clearly shows transferrin with a retention volume of 12.4 mL and the corresponding radioactive peak (Fig. 2). The small difference in the UV and radioactive peaks is due to the separation between the detectors within the FPLC system. It was discovered, and subsequently reported in the literature (*9*), that binding was possible both in the presence and the absence of bicarbonate as the synergistic anion. This step was omitted without

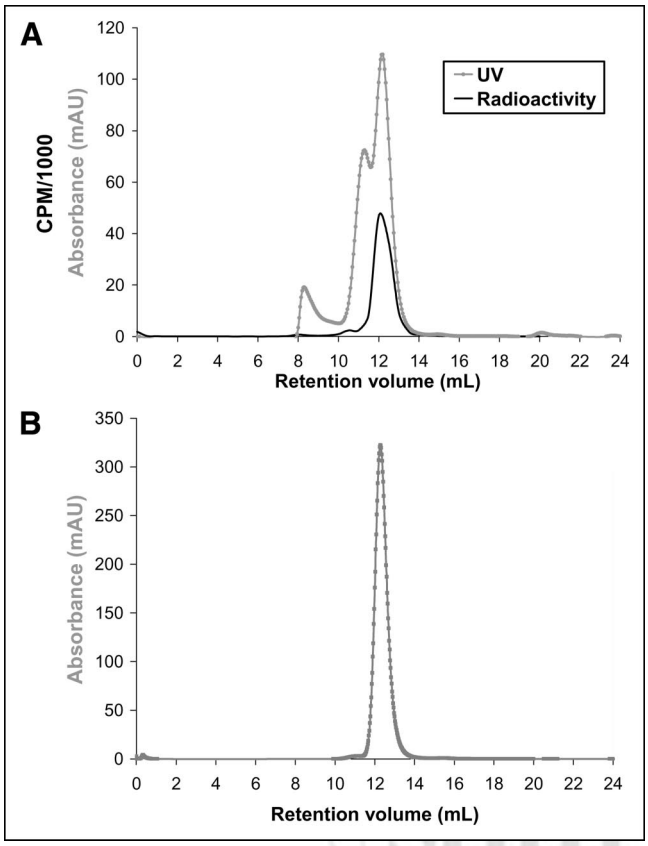

FIGURE 1. Radio-FPLC of rat serum 10 min after incubation with processed ^{45}Ti shows ^{45}Ti bound to a single protein (A) and FPLC of apotransferrin (B). mAU = milliabsorbance units.

consequence to simplify the procedure and remove any pH effect that could result from the addition of bicarbonate, a weak base.

A control experiment attempted ^{45}Ti binding to holotransferrin (iron-saturated transferrin) following the same methods as outlined for apotransferrin. Radio-FPLC analysis revealed no radioactive peak coeluting with the UV peak of transferrin, confirming no binding to the protein.

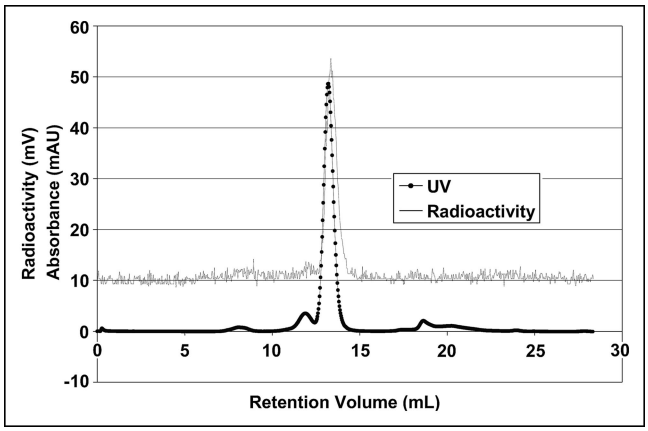

FIGURE 2. Radio-FPLC of ^{45}Ti-transferrin. mAU = milliabsorbance units.

Removal of low-molecular-weight impurities from the labeled ^{45}Ti-transferrin was initially achieved by elution through a PD-10 column containing prepacked Sephadex. This method effectively separated the protein fraction from any unbound ^{45}Ti but resulted in a large final solution volume of 3.5 mL. Protein separation from unbound ^{45}Ti and control over the final solution concentration was achieved through the use of a Centricon YM-30 filter tube. With a molecular weight cutoff of 30,000, any unbound ^{45}Ti was collected in the eluant fraction and the bound protein could be collected in a desired volume.

In vivo labeling of apotransferrin with ^{45}Ti was achieved by injection of ^{45}Ti-citrate. Radio-FPLC analysis of the ^{45}Ti-citrate showed a UV retention volume of 16 mL, concordant with the radioactive peak. Plasma analysis at 2 h after injection by radio-FPLC demonstrated that all ^{45}Ti was associated with transferrin in mouse plasma, with a retention volume of 12.4 mL and the corresponding radioactive peak.

Biodistribution

Tissue distribution of the processed ^{45}Ti was performed in normal, male Sprague–Dawley rats. As expected, the majority of the injected activity flooded the liver almost immediately (Table 1), accounting for almost 80% of the injected dose at both 10 min and 1 h. Spleen uptake was also considerably high and inhibitory for effective imaging of tumors.

The biodistribution of ^{45}Ti-transferrin in rats showed high initial retention in the blood with eventual washout by 24 h after injection (5.84 ± 0.43 %ID/g to 1.59 ± 0.37 %ID/g). Bone uptake increased over time, whereas lung uptake decreased. A comparison of the biodistribution of ^{45}Ti-transferrin with ^{67}Ga-citrate showed similar trends. The initial blood uptake was higher for the ^{45}Ti-transferrin, whereas bone uptake increased more for the ^{67}Ga-citrate (Tables 2 and 3).

In the rat biodistribution study, a plasma sample was taken at 4 h after injection and the plasma was analyzed by radio-FPLC to verify that the ^{45}Ti-transferrin remained intact. The radio-FPLC analysis showed a single radioactive peak with the same retention time as transferrin (Fig. 3).

TABLE 1
Biodistribution of $^{45}TiOCl_2$

Tissue	%ID/g ± SD	
	10 min	1 h
Blood	0.166 ± 0.032	0.145 ± 0.022
Lung	0.261 ± 0.031	0.192 ± 0.043
Liver	4.609 ± 0.870	4.700 ± 0.431
Spleen	7.274 ± 0.250	7.011 ± 3.150
Kidney	0.049 ± 0.009	0.051 ± 0.004
Muscle	0.003 ± 0.0004	0.004 ± 0.001
Fat	0.002 ± 0.001	0.003 ± 0.0005

n = 3 for each time point.

TABLE 2
Biodistribution of ^{45}Ti-Transferrin in Normal Rats

Tissue	%ID/g ± SD			
	10 min	2 h	4 h	7 h
Blood	5.85 ± 0.43	3.94 ± 0.66	2.01 ± 1.03	1.59 ± 0.37
Lung	2.39 ± 0.82	1.70 ± 0.40	1.17 ± 0.40	0.87 ± 0.24
Liver	1.55 ± 0.15	1.52 ± 0.17	1.35 ± 0.37	1.41 ± 0.10
Spleen	1.15 ± 0.18	0.95 ± 0.18	0.76 ± 0.23	0.74 ± 0.13
Kidney	1.41 ± 0.25	1.60 ± 0.21	1.39 ± 0.34	1.41 ± 0.15
Muscle	0.10 ± 0.03	0.18 ± 0.01	0.26 ± 0.05	0.26 ± 0.03
Fat	0.09 ± 0.02	0.18 ± 0.09	0.21 ± 0.05	0.23 ± 0.03
Heart	1.11 ± 0.11	1.09 ± 0.05	0.73 ± 0.21	0.56 ± 0.12
Brain	0.23 ± 0.03	0.17 ± 0.10	0.08 ± 0.04	0.10 ± 0.03
Bone (whole)	0.52 ± 0.10	1.09 ± 0.02	1.50 ± 0.20	1.97 ± 0.24

n = 4 for each time point.

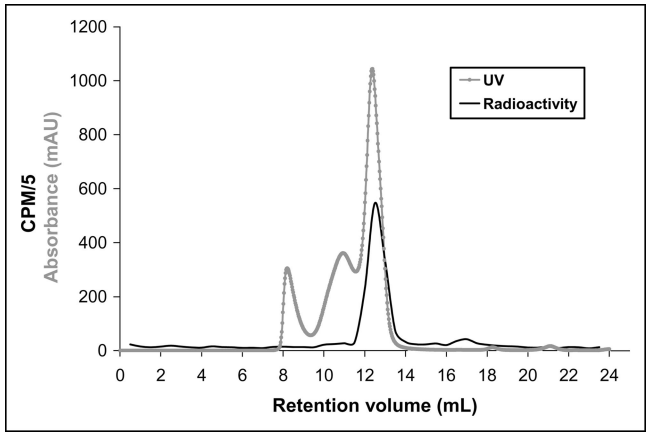

FIGURE 3. Radio-FPLC of serum from BALB/c mouse injected with ^{45}Ti-transferrin, 4 h after injection. mAU = milliabsorbance units.

The biodistribution of ^{45}Ti-transferrin in the EMT-6 tumor-bearing BALB/c mice showed initial blood uptake (37.2 ± 2.45 %ID/g) with washout by 24 h after injection (10.2 ± 1.03 %ID/g) ($P < 0.001$) (Table 4). Tumor uptake increased initially and was constant at ~15 %ID/g after 4 h. Tumor-to-muscle ratios were 3.41 ± 0.70 and 4.26 ± 0.67 at 4 and 24 h, respectively. ^{67}Ga (Table 5) cleared faster from the blood with higher bone uptake, and tumor uptake for ^{67}Ga was less than ^{45}Ti at ~8 %ID/g. However, the tumor-to-muscle ratio increased for ^{67}Ga from 4 to 24 h (3.14 ± 0.39 to 6.72 ± 1.18).

microPET

Two tumor models were imaged using microPET after intravenous injection of ^{45}Ti-transferrin. The EMT-6 mammary carcinoma tumor model showed distribution of ^{45}Ti throughout the heart, liver, kidneys, and tumor (Fig. 4). ROIs were defined around the 3 tumors in this mouse and used to calculate the SUVs, taking into account the decay-corrected injected dose and the animal's body weight. The large tumor on the left flank had a calculated SUV of 0.22 ± 0.01. The superior tumor on the right flank had an SUV of 0.21 ± 0.01, whereas the right inferior tumor had an SUV of 0.28 ± 0.01. By averaging all 3 tumor values, the overall SUV for the tumor was 0.24 ± 0.04. The SUV of the muscle (nontarget tissue) was 0.14 ± 0.01, resulting in a tumor-to-ratio of 1.68 ± 0.28.

The EMT-6 tumor model was also imaged in 6 mice after injection of ^{45}Ti-citrate (Fig. 5), which was proven to incorporate into transferrin by 2 h after injection. Quantitative analysis of ROIs drawn around the tumor in 5 of the mice at 2 and 4 h after injection gave average SUVs of 0.55 ± 0.04 and 0.55 ± 0.06, respectively. The SUVs for the nontarget tissue (muscle) were 0.32 ± 0.03 at 2 h and 0.39 ± 0.07 at 4 h after injection. Tumor-to-muscle ratios were then calculated to be 1.68 ± 0.41 at 2 h and 1.45 ± 0.30 at 4 h.

TABLE 3
Biodistribution of ^{67}Ga-Citrate in Normal Rats

Tissue	%ID/g ± SD			
	10 min	2 h	4 h	7 h
Blood	2.35 ± 1.22	1.38 ± 0.51	0.86 ± 0.74	0.64 ± 0.17
Lung	1.10 ± 0.48	0.64 ± 0.24	0.46 ± 0.28	0.34 ± 0.12
Liver	0.46 ± 0.25	0.56 ± 0.23	0.59 ± 0.34	0.61 ± 0.29
Spleen	0.41 ± 0.20	0.38 ± 0.18	0.31 ± 0.14	0.311 ± 0.16
Kidney	0.70 ± 0.25	0.56 ± 0.09	0.73 ± 0.26	0.66 ± 0.07
Muscle	0.22 ± 0.004	0.25 ± 0.03	0.21 ± 0.07	0.13 ± 0.02
Fat	0.13 ± 0.05	0.17 ± 0.01	0.13 ± 0.02	0.09 ± 0.01
Heart	0.79 ± 0.35	0.44 ± 0.10	0.27 ± 0.17	0.23 ± 0.06
Brain	0.09 ± 0.03	0.06 ± 0.04	0.04 ± 0.03	0.04 ± 0.01
Bone (whole)	0.67 ± 0.13	1.80 ± 0.13	3.02 ± 0.51	3.71 ± 0.04

n = 4 for each time point.

TABLE 4
Biodistribution of ^{45}Ti-Transferrin in BALB/c Mice Bearing EMT-6 Murine Mammary Carcinoma Tumors

Tissue	%ID/g ± SD		
	2 h	4 h	24 h
Blood	37.2 ± 2.45	32.3 ± 3.34	10.2 ± 1.03
Lung	13.2 ± 2.42	13.4 ± 0.50	
Liver	14.5 ± 1.57	17.3 ± 1.02	12.8 ± 0.58
Spleen	8.65 ± 1.71	11.0 ± 0.64	
Kidney	12.1 ± 1.61	11.8 ± 1.34	
Gallbladder	3.43 ± 2.25	3.08 ± 2.23	
Muscle	3.20 ± 0.29	4.28 ± 0.70	3.50 ± 0.37
Fat	3.93 ± 1.89	4.78 ± 0.70	
Heart	8.99 ± 0.84	9.51 ± 1.04	
Brain	1.13 ± 0.15	0.75 ± 0.04	
Bone (whole)	10.5 ± 0.63	15.2 ± 0.74	
Tumor	8.57 ± 2.04	14.6 ± 1.83	14.9 ± 1.74

n = 4 for each time point.

TABLE 5
Biodistribution of ^{67}Ga-Citrate in BALB/c Mice Bearing EMT-6 Murine Mammary Carcinoma Tumors

Tissue	%ID/g ± SD		
	2 h	4 h	24 h
Blood	15.8 ± 0.96	14.4 ± 0.68	2.77 ± 0.77
Lung	7.22 ± 0.50	7.27 ± 0.36	
Liver	5.71 ± 0.47	7.75 ± 0.41	7.31 ± 0.55
Spleen	4.77 ± 0.82	6.32 ± 0.72	
Kidney	5.97 ± 0.73	7.02 ± 0.75	
Gallbladder	2.88 ± 1.33	2.31 ± 0.89	
Muscle	2.97 ± 0.47	2.78 ± 0.15	1.08 ± 0.16
Fat	2.35 ± 0.57	2.22 ± 0.23	
Heart	4.25 ± 0.75	4.21 ± 0.34	
Brain	0.52 ± 0.10	0.47 ± 0.08	
Bone (whole)	10.3 ± 1.69	13.4 ± 0.86	
Tumor	7.05 ± 1.40	8.72 ± 0.98	7.26 ± 0.69

n = 4 for each time point.

DISCUSSION

Transferrin is known to be responsible for the selective delivery of gallium complexes to tumor cells (*17,28*), and transport of ^{45}Ti may also follow this pathway. With little known about the mechanism of action or the uptake pathway of titanium chemotherapeutics, PET using ^{45}Ti provides a biochemical view of this uptake along with the ability to quantitate accumulation.

The incorporation of ^{45}Ti into serum transferrin was demonstrated through both ex vivo and in vivo binding studies. The ex vivo labeling, during a brief (10 min) incubation period, provided proof of principle that titanium was able to bind transferrin, even when presented in an oxo-chloride form. Studies showed that after introduction in vivo as ^{45}Ti-transferrin and removal of plasma after 4 h, the complex remained intact. ^{45}Ti showed exclusive binding to transferrin in vivo, as illustrated by a single radioactive peak with the same retention volume as the serum transferrin peak.

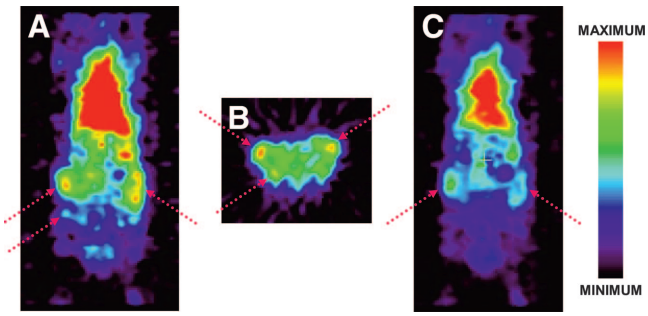

FIGURE 4. Two coronal microPET image slices (A and C) and 1 transaxial slice (B) of female BALB/c mouse bearing EMT-6 tumors (denoted by arrows) in both legs (right-hand side: 1 large tumor; left-hand side: 2 small tumors) injected with 27.72 MBq (750 μCi) ^{45}Ti-transferrin, 1 h 40 min after injection.

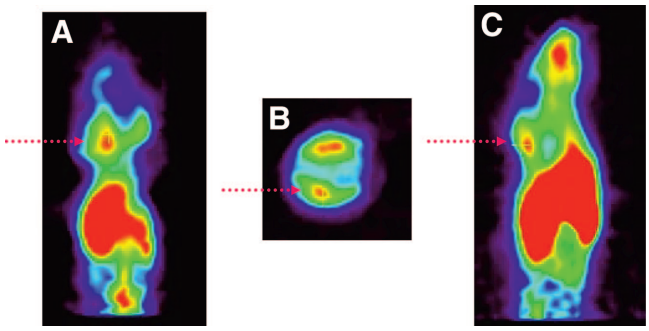

FIGURE 5. Coronal (A), transaxial (B), and sagittal (C) image slices of female BALB/c mouse bearing EMT-6 murine mammary carcinoma tumor (denoted by arrow) in nape of the neck injected with 7.59 MBq (205 μCi) ^{45}Ti-citrate, 2 h after injection.

A barrier to reproducible labeling was initially encountered. Although specific binding of ^{45}Ti to apotransferrin was observed, more than half of the radioactivity often remained adhered to the reaction vessel. To aid in the solubility of ^{45}Ti, 25 μmol/L ammonium citrate was added to the ^{45}Ti residue, resulting in ^{45}Ti-citrate as the injected imaging agent. Ti(IV)citrate has been shown as an appropriate complex for the incorporation of Ti^{4+} into apotransferrin in situ (*13,14*). Results demonstrated complete incorporation of ^{45}Ti into transferrin in vivo by 2 h after injection.

Several adjustments were made to the binding strategy of ^{45}Ti to apotransferrin. It was determined that efficient binding was obtained both with and without the presence of the carbonate anion typically necessary for iron binding. This is supported by a previous report that showed a delayed, but strong, binding of Ti(IV) to apotransferrin in the absence of bicarbonate. However, changes in structural conformation of the binding pocket were detected in each case (*9*). Fe(III) is bound in a distorted octahedral geometry with ligands provided by 4 amino acid side chains (2 tyrosines, 1 histidine, and 1 aspartic acid) and 2 oxygens from the synergistic bicarbonate anion. It is possible that the same amino acid ligands are coordinated to the metal center and the remaining coordination site is occupied by a double-bonded oxygen that most likely will not be removed on binding (Fig. 6). It is also possible that Ti^{4+} could adopt a 7-coordinate geometry, as demonstrated by complexes of Ti^{4+} with ethylenebis(o-hydroxyphenyl)glycine, a model ligand for the

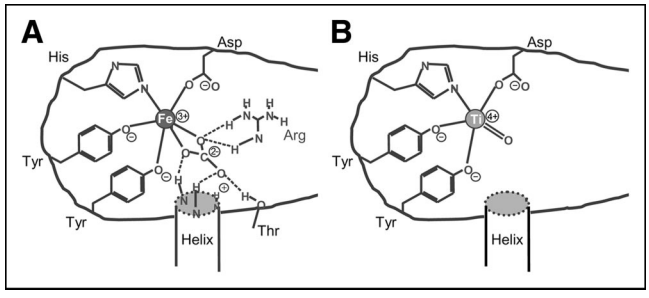

FIGURE 6. Schematic of iron (A) vs. titanium (B) (postulated) binding configurations.

binding site of transferrin (*29*). In this case, the Ti^{4+} assumes a pentagonal bipyramidal geometry with axial phenolate ligands, 2 amine nitrogens, 2 carboxylate oxygens, and the equatorial plane occupied by a H_2O ligand.

A Centricon purification step was added before labeling procedures and effectively improved reproducibility and labeling efficiency by removal of impurities that could potentially interact with the ^{45}Ti.

Biodistribution of the processed $^{45}TiOCl_2$ was rapid and occurred by almost exclusive localization in the liver and spleen. When normalized for %ID/organ, this resulted in >0% of the injected dose entering the liver by 10 min. As a result, incorporation of this nuclide into a complex will be essential for productive imaging due to its high nontarget tissue uptake.

A comparison of the biodistribution of ^{45}Ti-transferrin with that of ^{67}Ga-citrate showed similar trends in normal rats and in the tumor-bearing mouse model. The uptake values, however, were almost doubled in the ^{45}Ti-transferrin compared with the ^{67}Ga-citrate. Transchelation of ^{67}Ga into transferrin would be necessary and could delay uptake, whereas the ^{45}Ti was introduced as the transferrin complex. Increased levels of liver and bone uptake over time are most likely due to eventual uptake and trapping of the radionuclide by the numerous transferrin receptors in the liver and bone marrow. Tumor uptake in both cases was relatively high (14.6 ± 1.83 %ID/g for ^{45}Ti and 8.72 ± 0.98 %ID/g for ^{67}Ga) and remained elevated even out to 24 h after injection The tumor-to-muscle ratio of the ^{67}Ga-citrate reached 6.7 at 24 h, whereas the ^{45}Ti-transferrin ratio increased to 4.3 at this time point. An overall view of the trends and ratios observed in both biodistributions demonstrates that ^{45}Ti-transferrin may have a similar uptake pathway to ^{67}Ga-citrate, although complexities in the mechanism of uptake make direct comparison difficult.

Uptake of ^{45}Ti-transferrin was visualized the EMT-6 murine mammary carcinoma tumor model with microPET. Although the SUVs were not high (~0.5), in all cases, the tumor was clearly delineated from the surrounding tissue with tumor-to-muscle ratios on the order of 1.6. Comparison of the data suggests that tissue uptake is statistically similar whether injecting ^{45}Ti-transferrin directly or as ^{45}Ti-citrate, which transchelates to transferrin before the time of imaging.

Although this study was designed to aid in the elucidation of the mode of action of titanium anticancer agents, it also implicated ^{45}Ti-citrate as a possible clinical companion to ^{68}Ga-citrate with higher image resolution. ^{68}Ga has a maximum positron energy of 1.90 MeV, significantly higher than the 1.04-MeV positrons of ^{45}Ti, which would impart a lower dose to a patient. This difference in resolution could be especially beneficial for microPET, where image degradation is more apparent than in clinical scanners due to the higher intrinsic resolution of the instrument.

^{45}Ti-Transferrin has been established as a basis for comparison of the delivery of titanium chemotherapeutic agents. In the future, radiosynthetic techniques can be used to incorporate ^{45}Ti into anticancer drugs, which may actually be acting as prodrugs for the lethal effects of titanium alone, for direct comparison with ex vivo association of titanium into transferrin. The studies reported here clearly demonstrate the path of transport of titanium to tumor cells but do not specifically investigate the mechanism of action once delivered to the cell. Additional studies are currently being pursued by numerous groups to study the fate of titanium after entry into the cellular matrix.

CONCLUSION

^{45}Ti forms a complex with apotransferrin that remains intact in vivo. Results of the biodistribution in mice showed that the tumor had increased uptake compared with nontarget organs (e.g., muscle). Although blood uptake was initially high at 2 h, the levels dropped significantly at 24 h ($P < 0.001$). We also noted that the amount of activity found in the tumor remained constant between 4 and 24 h, a desirable property in radiopharmaceuticals for imaging. Images of tumor-bearing mice clearly delineate the tumors from the surrounding tissue, although the uptake in the 2 tumor types differed.

Biodistribution and microPET studies of ^{45}Ti-transferrin clearly demonstrate the transport of ^{45}Ti to tumors with uptake out to 24 h. This information forms a basis for the investigation of titanium radiopharmaceuticals and provides a tool for examining their mode of their transport to tumors.

ACKNOWLEDGMENTS

The authors thank Bill Margenau, Pat Margenau, Dave Ficke, and Todd Perkins for their technical help. Thanks also go to Michael R. Lewis, PhD, and Douglas J. Rowland, PhD, for their scientific contributions and to Jason S. Lewis, PhD, for his helpful discussions. This research was supported by the U.S. Department of Energy (grant DE-FG02-87ER60212). PET imaging was supported by a National Institutes of Health/National Cancer Institute (NIH/NCI) SAIRP grant (1 R24 CA083060) with additional support from the Small Animal Imaging Core of the Alvin J. Siteman Cancer Center at Washington University and Barnes-Jewish Hospital. The SAIC Core is supported by an NCI Cancer Center Support Grant (1 P30 CA091842).

REFERENCES

1. Kopf-Maier P, Kopf H. Organometallic titanium, vanadium, niobium, molybdenum and rhenium complexes: early transition metal antitumor drugs. In: Fricker SP, ed. *Metal Compounds in Cancer Therapy.* London, U.K.: Chapman and Hall; 1994:109–146.
2. Christodoulou CV, Ferry DR, Fyfe DW, et al. Phase I trial of weekly scheduling and pharmacokinetics of titanocene dichloride in patients with advanced cancer. *J Clin Oncol.* 1998;16:2761–2769.
3. Harding MM, Mokdsi G. Antitumor metallocenes: structure-activity studies and interactions with biomolecules. *Curr Med Chem.* 2000;7:1289–1303.
4. Koepf-Maier P, Koepf H. Non-platinum group metal antitumor agents: history, current status, and perspectives. *Chem Rev.* 1987;87:1137–1152.
5. Koepf-Maier P, Koepf H. Transition and main-group metal cyclopentadienyl

complexes: preclinical studies on a series of antitumor agents of different structural type. *Struct Bond (Berlin).* 1988;70:103–194.
6. Koepf-Maier P, Krahl D. Intracellular distribution of titanium after treatment with the antitumor agent titanocene dichloride: an electron energy loss spectroscopic study. *Naturwissenschaften.* 1981;68:273–274.
7. Koepf-Maier P, Wagner W, Liss E. Induction of cell arrest at G1/S and in G2 after treatment of Ehrlich ascites tumor cells with metallocene dichlorides and cis-platinum in vitro. *J Cancer Res Clin Oncol.* 1983;106:44–52.
8. Toney JH, Marks TJ. Hydrolysis chemistry of the metallocene dichlorides $M(\eta_5\text{-}C_5H_5)_2Cl_2$, M = titanium, vanadium, or zirconium: aqueous kinetics, equilibria, and mechanistic implications for a new class of antitumor agents. *J Am Chem Soc.* 1985;107:947–953.
9. Guo M, Sun H, McArdle HJ, Gambling L, Sadler PJ. Ti(IV) uptake and release by human serum transferrin and recognition of Ti(IV)-transferrin by cancer cells: understanding the mechanism of action of the anticancer drug titanocene dichloride. *Biochemistry.* 2000;39:10023–10033.
10. Faulk WP, Hsi BL, Stevens PJ. Transferrin and transferrin receptors in carcinoma of the breast. *Lancet.* 1980;316:390–392.
11. Panaccio M, Zalcberg JR, Thompson CH, et al. Heterogeneity of the human transferrin receptor and use of anti-transferrin receptor antibodies to detect tumours in vivo. *Immunol Cell Biol.* 1987;65:461–472.
12. Li H, Sadler PJ, Sun H. Rationalization of the strength of metal binding to human serum transferrin. *Eur J Biochem.* 1996;242:387–393.
13. Sun H, Li H, Weir RA, Sadler PJ. The first specific Ti^{IV}-protein complex: potential relevance to anticancer activity of titanocenes. *Angew Chem Int Edn Engl.* 1998;37:1577–1579.
14. Messori L, Orioli P, Banholzer V, Pais I, Zatta P. Formation of titanium(IV) transferrin by reaction of human serum apotransferrin with titanium complexes. *FEBS Lett.* 1999;442:157–161.
15. Kratz F, Hartmann M, Keppler B, Messori L. The binding properties of two antitumor ruthenium(III) complexes to apotransferrin. *J Biol Chem.* 1994;269:2581–2588.
16. Kratz F, Beyer U. Serum proteins as drug carriers of anticancer agents: a review. *Drug Deliv.* 1998;5:281–299.
17. Tsan MF, Scheffel U. Mechanism of gallium-67 accumulation in tumors. *J Nucl Med.* 1986;27:1215–1219.
18. Larson SM, Rasey JS, Allen DR, et al. Common pathway for tumor cell uptake of gallium-67 and iron-59 via a transferrin receptor. *J Natl Cancer Inst.* 1980;64:41–53.
19. Larson SM, Rasey JS, Allen DR. The transferrin-receptor hypothesis: mechanism of tumor uptake of carrier-free gallium-67. In: Horst W, Wagner HN Jr, Buchanan J, eds. *Frontiers in Nuclear Medicine.* Berlin, Germany: Springer-Verlag; 1980:134–153.
20. Rasey JS, Larson SM, Huebers H. Transferrin-mediated uptake of iron and gallium in three nonhematopoietic tumor cell lines. In: Saltman P, Hegenuer, J, eds. *The Biochemistry and Physiology of Iron: Proceedings of the 5th International Conference on Problems of Iron Storage and Transport, University of California, San Diego, Aug 24–26, 1981.* New York, NY: Elsevier; 1982:225–227.
21. Larson SM, Rasey JS, Allen DR, Grunbaum Z. A transferrin-mediated uptake of gallium-67 by EMT-6 sarcoma. II. Studies in vivo (BALB/c mice): concise communication. *J Nucl Med.* 1979;20:843–846.
22. Larson SM, Rasey JS, Allen DR, Nelson NJ. A transferrin-mediated uptake of gallium-67 by EMT-6 sarcoma. I. Studies in tissue culture. *J Nucl Med.* 1979;20:837–842.
23. Coleman RE. Single photon emission computed tomography and positron emission tomography in cancer imaging. *Cancer.* 1991;67:1261–1270.
24. Schuster DM, Alazraki N. Gallium and other agents in diseases of the lung. *Semin Nucl Med.* 2002;32:193–211.
25. Ishiwata K, Ido T, Monma M, et al. Potential radiopharmaceuticals labeled with titanium-45. *Appl Radiat Isot.* 1991;42:707–712.
26. Ishiwata K, Ido T, Monma M, et al. Preparation of ^{45}Ti-labeled compounds and their medical application. *J Labelled Compds Radiopharm.* 1982;19:11–12.
27. Vavere AL, Jones LR, McCarthy TJ, Rowland DJ, Welch MJ. Preparation, biodistribution, and microPET imaging of titanium-45-transferrin. *J Labelled Compds Radiopharm.* 2001;44:793–795.
28. Luttropp CA, Jackson JA, Jones BJ, Sohn M-H, Lynch RE, Morton KA. Uptake of gallium-67 in transfected cells and tumors absent or enriched in the transferrin receptor. *J Nucl Med.* 1998;39:1405–1411.
29. Guo M, Sun H, Bihari S, et al. Stereoselective formation of seven-coordinate titanium(IV) monomer and dimer complexes of ethylenebis(o-hydroxyphenyl) glycine. *Inorg Chem.* 2000;39:206–215.